Available online at www.sciencedirect.com
SCIENCE DIRECT®
International Journal of Heat and Fluid Flow 27 (2006) 696–706
International Journal of HEAT AND FLUID FLOW
www.elsevier.com/locate/ijhff

# Compressibility effects in the solenoidal dissipation rate equation: A priori assessment and modeling

Johannes Kreuzinger [a], Rainer Friedrich [a,*], Thomas B. Gatski [b]

[a] Fachgebiet Strömungsmechanik, Technische Universität München, D-85747 Garching, Germany
[b] Computational AeroSciences Branch, NASA Langley Research Center, Hampton, VA 23681-2199, USA

Available online 23 March 2006

**Abstract**

Several attempts have been made in the literature to improve the ability of statistical models to predict turbulent compressible flows. As yet, it is not possible to accurately predict both free and wall-bounded flows with the same model under a variety of conditions. One drawback in these attempts has been the lack of sufficiently reliable data with which to assess the various terms arising in the compressible turbulent transport equations. In this study, the exact terms of the solenoidal dissipation rate equation are calculated for the first time in both a compressible channel flow and a turbulent mixing layer. This data is then used to assess both the exact and modeled form of this equation. In its exact form, terms explicitly dependent on dilatation fluctuations and density and viscosity gradients appear. In addition, the terms that are also present in the incompressible equation now may vary differently under increased compressibility conditions. This latter effect can be either an indirect one, that is compressibility modifies mean quantities and Reynolds stresses, or a direct one, that is the processes in the solenoidal dissipation rate equation are themselves modified by compressibility. In order to separate the indirect and direct effects, it is assumed that the processes in the solenoidal dissipation rate equation are properly described by the available incompressible functional forms. The model coefficients are then determined by a priori tests. Direct effects appear if the coefficients depend on compressibility. These effects have then to be modeled additionally.


*Keywords:* Solenoidal dissipation rate equation; Direct numerical simulation; Compressibility effects; Modeling the baroclinic term

## 1. Introduction

Since the early 1990s, direct numerical simulations of compressible turbulent flows have become more common. These simulations increase our understanding of compressible turbulence, and aid in the development of turbulence models for compressible flows. For example, Blaisdell et al. (1993) have shown that compressibility effects in isotropic turbulence are highly dependent on initial conditions; whereas, in homogeneous turbulent shear flow compressibility effects become more or less independent of its initial conditions since the mean shear couples dilatation fluctuations with vorticity and strain rate fluctuations (a result demonstrated by linear theory). As a consequence, compressible isotropic turbulence is much less suited for turbulence model development than compressible homogeneous shear flow. Another important finding, resulting from DNS of homogeneous turbulent shear flow, has been reported by Sarkar (1995). It concerns the fact that the gradient Mach number, $M_g$, defined by the mean shear rate, an integral length scale and the mean speed of sound, controls the growth rate of turbulent kinetic energy (TKE) and not the turbulent Mach number. It also means that an increase in $M_g$ reduces the TKE production, and modifies the Reynolds stress anisotropy (structural changes). On the other hand, related changes in pressure–dilatation correlation and compressible dissipation rate (energetic effects) are comparatively weak up to supersonic $M_g$ numbers. Hence, turbulence models for compressible flow have

* Corresponding author. Tel.: +49 89 2891 6144; fax: +49 89 2891 6145.
*E-mail addresses:* r.friedrich@lrz.tum.de (R. Friedrich), t.b.gatski@larc.nasa.gov (T.B. Gatski).

0142-727X/$ - see front matter © 2006 Elsevier Inc. All rights reserved.
doi:10.1016/j.ijheatfluidflow.2006.02.014

**Nomenclature**

$B_\varepsilon$ baroclinic term, Eq. (6i) ($m^2/s^4$)
$c_p$, $c_v$ specific heats at constant pressure and volume ($m^2/(s^2\,K)$)
$C^1_\varepsilon$, $C^2_\varepsilon$, $C^3_1$, $C^3_2$ coefficients in the turbulence models for production and destruction terms (–)
$C_\mu$ coefficient in the model for turbulent transport term (–)
$C_\rho$, $C_p$, $C_{p\rho}$, $C_{B_\varepsilon}$ coefficients in the turbulence model for baroclinic term (–)
$C^{SC}_\varepsilon$ term (7c) defined by Sinha and Candler (2003) ($m^2/s^4$)
$D_\varepsilon$ viscous diffusion term, Eq. (6g) ($m^2/s^4$)
$D^{SC}_\varepsilon$ term (7a) defined by Sinha and Candler (2003) ($m^2/s^4$)
$F_\varepsilon$ term (6j) involving cross-products between density and viscous stress gradients ($m^2/s^4$)
$H$ channel half width (m)
$K = \frac{1}{2}\overline{\rho u_i'' u_i''}/\bar\rho$ specific turbulent kinetic energy ($m^2/s^2$)
$l = (2K)^{3/2}/\varepsilon$ integral turbulent length scale (m)
$M = u_{av}/c_w$ global Mach number, channel flow
$M_c = \Delta u/(c_1 + c_2)$ convective Mach number, mixing layer
$p$ pressure ($kg/(m\,s^2)$)
$Pr = \mu c_p/\lambda_T$ Prandtl number
$P^1_\varepsilon$, $P^2_\varepsilon$, $P^3_\varepsilon$, $P^4_\varepsilon$ production terms, Eqs. (6a)–(6d) ($m^2/s^4$)
$Re_{av} = \rho_{av} u_{av} H/\mu_{av}$ global Reynolds number, channel flow
$Re_l = \frac{\sqrt{2K}l}{\nu}$ turbulent Reynolds number
$Re_\theta = \rho_{av}\Delta u \delta_\theta/\mu_{av}$ global Reynolds number, mixing layer
$Re_\lambda = \frac{\sqrt{2K}\lambda}{\nu}$ Taylor Reynolds number
$s_{ij} = \frac{1}{2}(u_{i,j} + u_{j,i})$ strain rate tensor (1/s)
$S^* = \frac{|\nabla\overline{U}|K}{\varepsilon}$ non-dimensional shear rate
$T$ temperature (K)
$T_\varepsilon$ turbulent transport term, Eq. (6f) ($m^2/s^4$)
$T^c_\varepsilon$ compressible turbulent transport term, Eq. (6h) ($m^2/s^4$)
$u_i$ Cartesian component of velocity vector (m/s)
$\widetilde{u_i'' u_j''} = \overline{\rho u_i'' u_j''}/\bar\rho$ specific Reynolds stress ($m^2/s^4$)
$u_\tau = \sqrt{\tau_w/\rho_w}$ shear stress velocity (m/s)
$u^*_\tau = \sqrt{\tau_w/\bar\rho}$ semi-local shear stress velocity (m/s)
$z$ Cartesian coordinate, normal to wall or in main shear direction (m)
$z^* = z\bar\rho u^*_\tau/\bar\mu$ semi-local viscous coordinate (–)

*Greek symbols*
$\gamma = c_p/c_v$ ratio of specific heats
$\delta_\theta$ momentum thickness (m)
$\delta_{ij}$ Kronecker delta (–)
$\varepsilon_s, \varepsilon_d, \varepsilon_I$ solenoidal, dilatational and inhomogeneous dissipation rates, respectively, Eqs. (4a)–(4c) ($m^2/s^3$)
$\zeta = z/\delta_\theta$ non-dimensional Cartesian coordinate (–)
$\lambda = \sqrt{\frac{\nu 2K}{\varepsilon}}$ Taylor micro scale (m)
$\lambda_T$ heat conduction coefficient ($m\,kg/(s^3\,K)$)
$\mu$ dynamic viscosity ($kg/(m\,s)$)
$\nu$ kinematic viscosity ($m^2/s$)
$\rho$ density ($kg/m^3$)
$\sigma_\epsilon$ constant model coefficient, $\sigma_\epsilon = 1.3$
$\tau_{ij} = 2\mu(s_{ij} - \frac{1}{3}s_{kk}\delta_{ij})$ Cartesian component of viscous stress tensor ($kg/(m\,s^2)$)
$\tau_w$ wall shear stress ($kg/(m\,s^2)$)
$\Upsilon$ viscous destruction term, Eq. (6e) ($m^2/s^4$)
$\Upsilon^{SC}$ viscous destruction term as defined by Sinha and Candler (2003), Eq. (7b) ($m^2/s^4$)
$\phi, \phi_1, \phi_2, \phi_3$, dissipation rate of $K$ and parts of it, Eqs. (1), (2a)–(2c) ($kg/(m\,s^3)$)
$\omega_i$ Cartesian component of vorticity vector (1/s)

primarily to account for structural changes in the Reynolds stress tensor. Inspection of the Reynolds stress transport equations immediately leads to the realization that such structural changes will be due to the source/sink terms in these equations, namely production, pressure–strain rate correlation and turbulent dissipation rate. Such structural changes have also been demonstrated by Simone et al. (1997) using linear rapid-distortion theory. Their RDT analysis was capable of predicting the TKE growth rate and the Reynolds shear stress anisotropy in surprisingly close agreement with DNS data.

In direct simulations of high-speed mixing layers, Pantano and Sarkar (2002) observed a monotone decrease of the normalized pressure–strain rate correlation with increasing convective Mach number that directly translated into an inhibited energy transfer from the stream-wise to the cross-stream Reynolds stresses. They also confirmed the key role of the gradient Mach number in determining the reduction of the pressure–strain rate term and provided a rigorous explanation of this effect based on a wave equation for the pressure. A different mechanism is responsible for similar changes in the structure of the pressure–strain rate tensor in compressible flow along cooled walls. Based on DNS data of supersonic channel flow and a Green's function analysis of the pressure Poisson equation, Foysi et al. (2004) found mean density variations normal to the wall (due to kinetic energy dissipation) to be responsible for the reduction of pressure–strain rate correlations.

Unlike compressibility related changes of the Reynolds stress tensor, corresponding changes of the turbulent dissipation rate tensor have not been investigated so far using DNS data. To the best of our knowledge, the only attempt

to use DNS data of compressible flow to analyze the solenoidal part of the TKE dissipation rate $\varepsilon_s$ is that of Sinha and Candler (2003). They analyzed all the terms in the $\varepsilon_s$-equation in the case of a Mach 4 turbulent boundary layer as well as highlighted similarities and differences of the terms with respect to the incompressible case and discussed modeling implications. Previous studies of modeling the dissipation rate equation ($\varepsilon$-equation) have focused on incompressible flows using DNS databases. Mansour et al. (1988) were the first to identify the different terms in the $\varepsilon$-equation and to note that existing closure models work well away from the wall, but need improvement close to the wall. Rodi and Mansour (1993) provided improved models for production, destruction, turbulent diffusion and pressure diffusion in the $\varepsilon$-equation, using channel DNS-data of Kim et al. (1987). Nagano and Shimada (1995) provided a new and rigorous model for both the TKE and the $\varepsilon$-equation that not only improved the Rodi and Mansour channel flow predictions, but also showed excellent results in ZPG and APG boundary layer predictions compared to DNS and experimental data. As the present results will reveal, excellent low Reynolds number turbulence models for incompressible flow form the basis for proper compressible flow modeling for wall-bounded flows, and that fairly simple adaptions of incompressible model forms are suited for compressible flow predictions.

Motivated by the above, the analysis here starts from the exact transport equation for the solenoidal part of the TKE dissipation rate, and utilizes a natural splitting into a viscous diffusion, destruction and a volume force term normal to the density gradient that contrasts with that of Sinha and Candler (2003). Incompressible models for production, destruction and turbulent transport terms are then adapted to compressible flow by introducing the local mean density, viscosity, and Favre averaged quantities. An a priori assessment of the models consists of determining the model coefficients from DNS of the exact terms and the model functions. This is done separately for channel flow and mixing layer, showing that the model coefficients are independent of Mach number. In the low-speed mixing layer, density variations need separate modeling. A new model is proposed for the baroclinic term in the $\varepsilon_s$-equation.

## 2. Exact and modeled form of the solenoidal dissipation rate equation

It has been shown by Huang et al. (1995) that the turbulent kinetic energy dissipation rate $\phi = \overline{\tau'_{ij}u'_{i,j}}$ can be decomposed into terms involving correlation between fluctuations of the deformation tensor $s_{ij} = \frac{1}{2}(u_{i,j} + u_{j,i})$ and terms involving correlations between fluctuations of viscosity and $s'_{ij}$, namely:

$$\phi = \overline{\tau'_{ij}u'_{i,j}} = \phi_1 + \phi_2 + \phi_3, \tag{1}$$

where

$$\phi_1 = 2\bar{\mu}\overline{s'_{ij}s'_{ij}} - \frac{2}{3}\bar{\mu}\overline{s'_{kk}s'_{ll}}, \tag{2a}$$

$$\phi_2 = 2\overline{\mu' s'_{ij}s'_{ij}} - \frac{2}{3}\overline{\mu' s'_{kk}s'_{ll}}, \tag{2b}$$

$$\phi_3 = 2\overline{\mu' s'_{ij}}\,\overline{s_{ij}} - \frac{2}{3}\overline{\mu' s'_{kk}}\,\overline{s_{ll}}. \tag{2c}$$

In these and the following expressions, a single prime $(\cdot)'$ denotes a Reynolds fluctuation. The quantity $\phi_1$ can again be expressed as the sum of three parts: the solenoidal and dilatational dissipation rates and an inhomogeneous term

$$\phi_1 = \bar{\rho}(\varepsilon_s + \varepsilon_d + \varepsilon_I) \tag{3}$$

with

$$\varepsilon_s = \tilde{\nu}\overline{\omega'_i\omega'_i}, \tag{4a}$$

$$\varepsilon_d = \frac{4}{3}\tilde{\nu}\overline{s'_{kk}s'_{ll}}, \tag{4b}$$

$$\varepsilon_I = 2\tilde{\nu}\Big(\big(\overline{u'_i u'_j}\big)_{,ij} - 2\big(\overline{u'_i u'_{j,j}}\big)_{,i}\Big). \tag{4c}$$

Using the DNS data of Coleman et al. (1995), Huang et al. (1995) have demonstrated that correlations involving viscosity fluctuations (terms $\phi_2$ and $\phi_3$) and the compressible dissipation rate $\bar{\rho}\varepsilon_d$ are negligibly small in supersonic channel flow at least up to global Mach numbers of 3. Hence, the solenoidal dissipation rate $\bar{\rho}\varepsilon_s$ and the inhomogeneous term $\bar{\rho}\varepsilon_I$ are the terms dominating dissipation effects in the turbulent kinetic energy equation. Our interest lies in the transport equation for $\varepsilon_s$. The inhomogeneous term $\bar{\rho}\varepsilon_I$ is dominated by the second derivative of the Reynolds stresses, hence its specification is a question of Reynolds stress modeling. For this study, the $\varepsilon_s$-equation is written in the form

$$\frac{\mathrm{D}\varepsilon_s}{\mathrm{D}t} = P^1_\varepsilon + P^2_\varepsilon + P^3_\varepsilon + P^4_\varepsilon + T_\varepsilon + D_\varepsilon - \Upsilon + F_\varepsilon + T^c_\varepsilon + B_\varepsilon + \frac{\varepsilon_s}{\tilde{\nu}}\frac{\mathrm{D}\tilde{\nu}}{\mathrm{D}t}. \tag{5}$$

In Eq. (5)

$$P^1_\varepsilon = -2\tilde{\nu}\overline{(u'_{i,j} - u'_{j,i})u'_{k,j}}\bar{u}_{i,k}, \tag{6a}$$

$$P^2_\varepsilon = -2\tilde{\nu}\overline{(u'_{i,j} - u'_{j,i})u'_{i,k}}\bar{u}_{k,j} \tag{6b}$$

are the turbulent production of dissipation due to mean velocity gradients,

$$P^3_\varepsilon = -2\tilde{\nu}\overline{(u'_{i,j} - u'_{j,i})u'_k}\bar{u}_{i,jk} = -2\tilde{\nu}\overline{\omega'_i u'_k}\bar{\omega}_{i,k} \tag{6c}$$

is the production due to the mean vorticity gradient,

$$P^4_\varepsilon = -2\tilde{\nu}\overline{(u'_{i,j} - u'_{j,i})u'_{i,k}u'_{k,j}} \tag{6d}$$

is the production due to vortex stretching by fluctuating velocity gradients and

$$-\Upsilon = -2\tilde{\nu}\overline{\big((u'_{i,j} - u'_{j,i})/\rho\big)_{,k}\tau_{ik,j}} \tag{6e}$$

is the viscous destruction term.

$$T_\varepsilon = -\tilde{\nu}\left(\overline{u'_k(u'_{i,j}-u'_{j,i})u'_{i,j}}\right)_{,k} \tag{6f}$$

and

$$D_\varepsilon = 2\tilde{\nu}\left(\overline{(u'_{i,j}-u'_{j,i})\frac{1}{\rho}\tau_{ik,j}}\right)_{,k} \tag{6g}$$

are the turbulent transport and viscous diffusion terms. The remaining terms constitute the explicit contributions of compressibility or density and viscosity gradients. These include

$$T^{c}_\varepsilon = \tilde{\nu}\overline{(u'_{i,j}-u'_{j,i})u'_{i,j}u'_{k,k}}, \tag{6h}$$

which is the compressible turbulent transport,

$$B_\varepsilon = 2\tilde{\nu}\overline{(u'_{i,j}-u'_{j,i})\rho_{,j}p_{,i}/\rho^2} \tag{6i}$$

and

$$F_\varepsilon = -2\tilde{\nu}\overline{(u'_{i,j}-u'_{j,i})\rho_{,j}\tau_{ik,k}/\rho^2}, \tag{6j}$$

which are the contributions due to forces on a volume element that are normal to the density gradient. The baroclinic term $B_\varepsilon$ is due to the force exerted by the pressure gradient, $F_\varepsilon$ is due to the force resulting from the viscous stress gradient. The last term on the RHS of Eq. (5) requires no modeling and is simply the variation of the mean kinematic viscosity. In the cases to be examined here, this term can be neglected.

In the recent study by Sinha and Candler (2003), their $\varepsilon_s$-equations differs from the one used here in the partitioning of terms originating from the viscous term in the momentum equation. They obtained a viscous diffusion term, $D^{SC}_\varepsilon$, a viscous destruction term, $\Upsilon^{SC}$, and a viscosity variation term, $C^{SC}_\varepsilon$, that can be written as

$$D^{SC}_\varepsilon = \tilde{\nu}^2\overline{\left(u'_{i,j}u'_{i,j}-u'_{i,j}u'_{j,i}\right)}_{,kk}, \tag{7a}$$

$$-\Upsilon^{SC} = -2\tilde{\nu}^2\overline{(u'_{i,j}-u'_{j,i})_{,k}u'_{i,jk}}, \tag{7b}$$

$$C^{SC}_\varepsilon = -\Upsilon + D_\varepsilon + F_\varepsilon + \frac{\varepsilon_s}{\tilde{\nu}}\frac{D\tilde{\nu}}{Dt} - D^{SC}_\varepsilon + \Upsilon^{SC}_\varepsilon. \tag{7c}$$

$\Upsilon^{SC}$ and $D^{SC}_\varepsilon$ are the terms that appear in the case of incompressible flow with no property variation, and all effects of compressibility and property variation are contained in $C^{SC}_\varepsilon$. This makes the term $C^{SC}_\varepsilon$ difficult to interpret. In the limit of incompressible flow with no mean property variations, both formulations are equivalent, that is $F_\varepsilon \to 0, C^{SC}_\varepsilon \to 0, \Upsilon \to \Upsilon^{SC}$ and $D_\varepsilon \to D^{SC}_\varepsilon$. This is not the case in flows with high density and viscosity gradients. As an example, Fig. 1 shows the magnitude of the terms used by Sinha and Candler (2003) in channel flow at $M = 3.1$ (case K6000n, Table 1). $C^{SC}_\varepsilon$ and $D^{SC}_\varepsilon$ are in balance at the wall, and each term has high values that reach three times the maximum of the destruction term $\Upsilon^{SC}$. Using the partitioning presented here, no such large terms arise (Fig. 2). The term additionally appearing compared to the incompressible equation, $F_\varepsilon$, remains negligible. Figs. 3 and 4 show that the terms used here behave qualitatively the same for a wide range of Mach numbers. This suggests

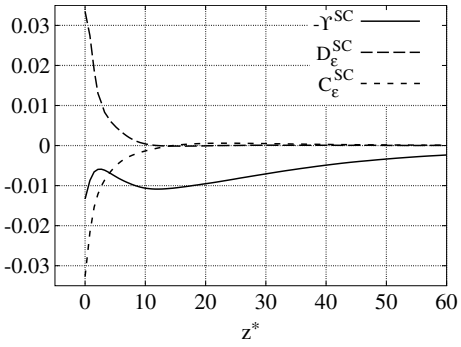


Fig. 1. Terms derived by Sinha and Candler (2003), Eqs. (7a)–(7c); Channel flow K6000n, semi-local scaling by $\tau_w^3/\bar{\mu}^2/\bar{\rho}$.

Table 1
Parameters of the DNS of channel flow with cooled walls

| Flow case | $M = \frac{u_{av}}{c_w}$ | $Re_{av} = \frac{\rho_{av}u_{av}H}{\mu_{av}}$ |
|---|---|---|
| KM03 | 0.350 | 2808.6 |
| K3000 | 1.5327 | 2452.2 |
| K6000n | 3.1399 | 3204.0 |

$H$ is the channel half width, the subscript av denotes values averaged over the whole flow domain, w wall values.

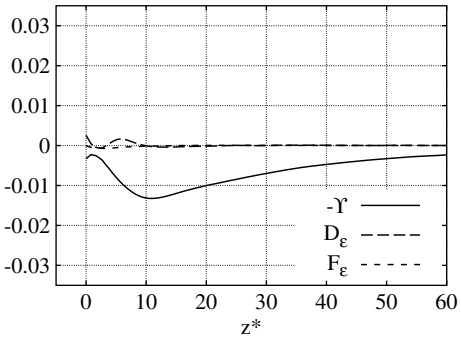


Fig. 2. Terms used in the present study, Eqs. (6e), (6g) and (6j); channel flow K6000n, semi-local scaling by $\tau_w^3/\bar{\mu}^2/\bar{\rho}$.

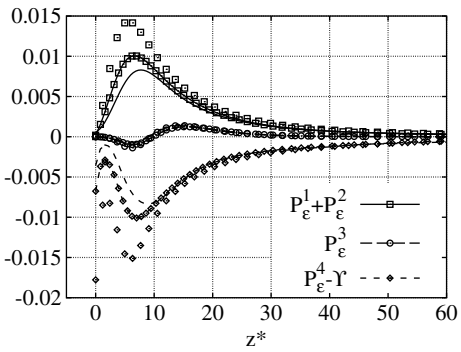


Fig. 3. Production and destruction terms in the $\varepsilon_s$-equation; channel flow at different Mach numbers, KM03 (symbols), K3000 (lines and symbols) and K6000n (lines), semi-local scaling by $\tau_w^3/\bar{\mu}^2/\bar{\rho}$.

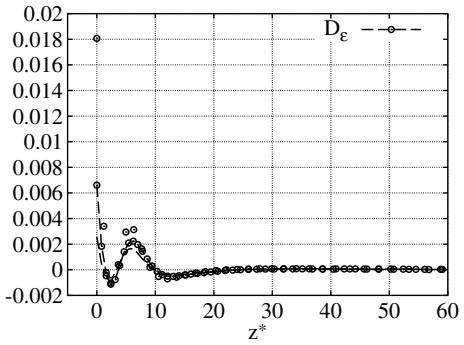


Fig. 4. Viscous diffusion term in the $\varepsilon_s$-equation; channel flow at different Mach numbers, KM03 (symbols), K3000 (lines and symbols) and K6000n (lines), semi-local scaling by $\tau_w^3/\bar{\mu}^2/\bar{\rho}$.

that the high values of $C_\varepsilon^{SC}$ and $D_\varepsilon^{SC}$ seem to result from an unphysical split of small terms.

Models are needed to close the production, destruction and transport terms in Eq. (5). These are given by

$$P_\varepsilon^1 + P_\varepsilon^2 = -C_\varepsilon^1 \frac{\varepsilon_s}{K} \widetilde{u_i'' u_j''}\, \widetilde{U}_{i,j}, \tag{8}$$

$$P_\varepsilon^4 - \Upsilon = -C_\varepsilon^2 \varepsilon^2/K, \tag{9}$$

$$P_\varepsilon^3 = -C_1^3 \cdot \tilde{\nu} C_\mu \frac{K^2}{\varepsilon} \widetilde{U}_{i,kk}^2 - C_2^3 \cdot \tilde{\nu} \frac{K}{\bar{\rho}\varepsilon} (\bar{\rho}K)_{,m} \widetilde{U}_{i,m} \widetilde{U}_{i,kk}, \tag{10}$$

$$T_\varepsilon = f_t \cdot \left[ \frac{C_\mu}{\sigma_\varepsilon} \frac{\bar{\rho}K^2}{\varepsilon} (\bar{\rho}\varepsilon)_{,i} \right]_{,i} \Big/ \bar{\rho}^2, \tag{11}$$

where $C_\mu$ is defined by $-\widetilde{u_i'' u_j''} = C_\mu (K^2/\varepsilon) \widetilde{U}_{i,j}$. The models for Eqs. (8) and (9) were originally proposed by Hanjalić and Launder (1972), and the model for $P_\varepsilon^3$ was developed by Rodi and Mansour (1993). The turbulent transport $T_\varepsilon$ is modeled by a gradient diffusion model with $\sigma_\varepsilon = 1.3$. All these models were designed for incompressible flow and are adapted here for compressible flow by introducing variable density and viscosity, and Favre mean and fluctuating quantities. In the partitioning used here, the viscous diffusion term $D_\varepsilon$ is not closed and it also has to be modeled.

The above models are used for a priori tests. From the DNS simulations, each quantity in the above equations is known, and the model coefficients $C_\varepsilon^1$, $C_\varepsilon^2$, $C_1^3$, $C_2^3$, $f_t$, and $C_\mu$ can be determined. When these coefficients are calculated from DNS data, compressibility effects altering these quantities can be identified. The cases of channel flow and mixing layer will be studied separately. This will isolate the effects of compressibility in wall bounded and free shear flows.

All the direct simulations are performed using a finite-difference scheme for the primitive variables pressure, velocity and entropy. Integration in time is done by a third order Runge–Kutta scheme. Two different spatial discretizations are used: A fifth order compact upwind scheme in the case of channel flows, and an optimized fourth order central compact scheme plus filtering of the highest wavenumbers to stabilize the simulations in the case of the mixing layer. A grid study in DNS of homogeneous sheared turbulence showed that the terms in the $\varepsilon_s$-equation (5) can be claimed to be converged, if the error in this balance equation is smaller than 20% of the destruction term $\Upsilon$ and if $\Upsilon$ itself is not calculated explicitly, but as the sum of all terms (Kreuzinger, 2006). This condition is met in the channel and mixing layer simulations. The necessary numerical meshes contained up to 27 and 134 million grid points in the channel, respectively the mixing layer case.

## 3. Compressibility effects and their modeling

In order to properly compare terms and model coefficients for the various Mach and Reynolds numbers, suitable scaling parameters have to be found. For the turbulent channel flow data analyzed here, Foysi et al. (2004) have successfully used $u_\tau^* = \sqrt{\tau_w/\bar{\rho}}$ as a fluctuating velocity scale, and $\bar{\mu}/\tau_w$ and $H/u_{av}$ ($u_{av}$ = volume averaged mean velocity) as the proper time scales for the near-wall and the core regions, respectively. This allows for the scaling of all the terms in the $\varepsilon_s$-equation that can then be plotted against the semi-local viscous coordinate $z^* = z\bar{\rho}u_\tau^*/\bar{\mu} = z\sqrt{\bar{\rho}\tau_w}/\bar{\mu}$, close to the wall, and against $z/H$ in the core region. In the mixing layer, one scaling is sufficient throughout the flow, namely $\Delta u$ (velocity difference across the layer) for the velocity fluctuations, and $\delta_\theta/\Delta u$ for the timescale ($\delta_\theta$ = momentum thickness). The relevant coordinate there is the self-similar coordinate $\zeta = z/\delta_\theta$.

### 3.1. Channel flow

Channel flow simulations carried out by Foysi et al. (2004) are used here. The three channel flows (see Table 1) cover a substantial range of Mach numbers. The Reynolds number, defined from mean quantities, $Re_{av}$ varies little between cases. In the definitions $M = \frac{u_{av}}{c_w}$ and $Re_{av} = \frac{\rho_{av} u_{av} H}{\mu_{av}}$, volume averaged quantities are defined by integration across the channel, e.g. $\rho_{av} = \int_0^1 \bar{\rho}\, \mathrm{d}(z/H)$. In all cases, the Prandtl number and the ratio of specific heats are kept at constant values, $Pr = 0.71$, $\gamma = 1.4$, and the viscosity follows the power law $\mu \sim T^{0.7}$. The main effect of increasing Mach number is to increase the mean property variation in the range $z^* < 30$. This region is characterized by steep gradients of density and viscosity close to the cooled wall. For the three Mach number cases simulated, the wall density is 0.02, 0.37 and 1.54 times higher than the mean density. This effect is proportional to $M^2$. In addition, any differences in mean velocity between the different cases are accounted for using the channel flow velocity scalings.

The near-wall scaling collapses the positions of the peaks of terms in the $\varepsilon_s$-equation (5), but the amplitudes show a monotonic decrease with increasing Mach number (Fig. 3). Only the terms explicitly dependent on compressibility or density and viscosity gradients $T_\varepsilon^c$, $B_\varepsilon$ and $F_\varepsilon$ increase with Mach number, but they still remain negligible. Their maximum amplitude reaches 0.00075 in semi-local scaling, which is less than one-tenth of the dominant

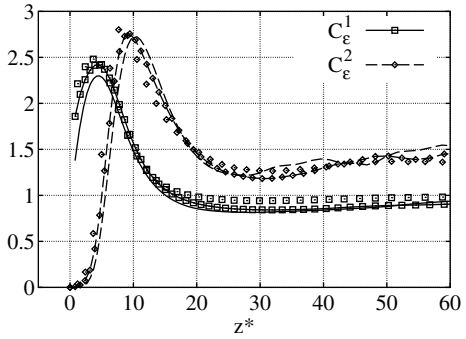


Fig. 5. Model coefficient $C_\varepsilon^1$ and $C_\varepsilon^2$ variation across channel at different Mach numbers; KM03 (symbols), K3000 (lines and symbols) and K6000n (lines).

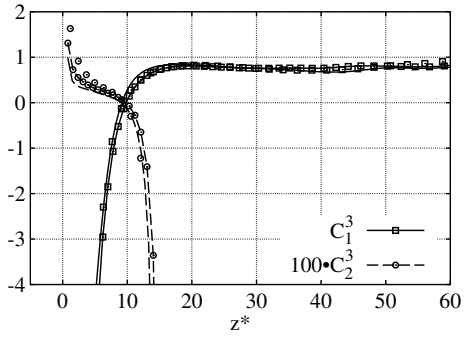


Fig. 6. Model coefficient $C_1^3$ and $C_2^3$ variation across channel at different Mach numbers; KM03 (symbols), K3000 (lines and symbols) and K6000n (lines).

terms.[1] At the wall, the viscous diffusion term $D_\varepsilon$ decreases with increasing Mach number (Fig. 4). For $z^* > 30$ no compressibility effect was seen (a result confirmed using an outer scaling for the center region of the channel).

Plotted in inner variables, the profiles of the coefficients $C_\varepsilon^1$ and $C_\varepsilon^2$ for the different Mach numbers collapse (see Fig. 5). This indicates that no compressibility effects influence either the production or destruction terms.

Unfortunately, evaluation of the models for $P_\varepsilon^3$ and $T_\varepsilon$ is more difficult since these terms change sign across the channel. Some progress can be made, however, by examining each term of the model for $P_\varepsilon^3$ separately (see Eq. (10)). Fig. 6 shows that the second term is only important near the wall ($z^* < 12$). This is exemplified by the relatively constant values of both $C_1^3$ and $C_2^3$ (≈0.7 and 0.007, respectively) in their respective regions of importance. $C_1^3$ shows no dependence on Mach number, $C_2^3$ is decreasing, but only slightly.

For the transport $T_\varepsilon$, there is a relatively good collapse of the data for the model coefficient $f_t$ in the regions shown

[1] The evaluation of the data of a compressible boundary layer at $M = 2.25$ (Pirozzoli et al., 2004) showed that the terms which explicitly depend on compressibility or density and viscosity gradients, reach amplitudes of 0.00085. So they are also negligible near adiabatic walls.

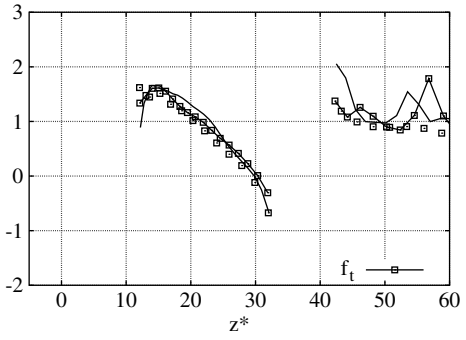


Fig. 7. Model coefficient $f_t$ variation across channel at different Mach numbers; KM03 (symbols), K3000 (lines and symbols) and K6000n (lines).

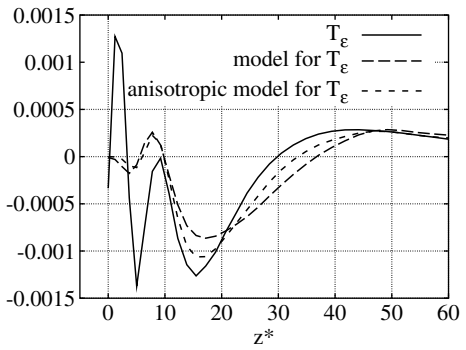


Fig. 8. Turbulent transport of $\varepsilon_s$, channel flow at low Mach number KM03 (–) $T_\varepsilon$; (––) model Eq. (11), $f_t = 1.0$; (- - -): 0.18. $[\bar{\rho}\widetilde{u_i''u_j''}\frac{K}{\varepsilon_s}(\bar{\rho}\varepsilon_s)_{,j}]_{,i}/\bar{\rho}^2$; semi-local scaling by $\tau_w^3/\bar{\mu}^2/\bar{\rho}$.

in Fig. 7. In the near-wall region ($z^* < 12$) and in the region $32 < z^* < 42$ (not shown), $T_\varepsilon$ changes sign, so no meaningful value of the coefficient can be obtained. If directly compared to the exact term, the model works well except for a small region in close proximity to the wall (Fig. 8). An improvement of the model is possible, if the dependence on turbulent kinetic energy is replaced by individual Reynolds stress components.

In incompressible flows, the viscous diffusion term $D_\varepsilon$ equals $(\nu\varepsilon_{,i})_{,i}$. This relation can be adapted directly to compressible flows by introducing a variable density and viscosity. This leads to $D_\varepsilon \approx (\bar{\mu}(\bar{\rho}\varepsilon)_{,i})_{,i}/\bar{\rho}^2$ (Model A). A more general and more complex expression can be obtained using the fact, that – except for the wall point – in semi-local scaling the term is nearly independent of compressibility (Fig. 4). Since this is also true for the solenoidal dissipation rate in semi-local scaling, the relation $D_\varepsilon^* \approx \partial^2\varepsilon^*/\partial z^{*2}$, which is exact as Mach number goes to zero, can be used as a model. Here the semi-locally normalized quantities are $D_\varepsilon^* = D_\varepsilon/(\tau_w^3/\bar{\mu}^2/\bar{\rho})$, $\varepsilon^* = \varepsilon/(\tau_w^2/\bar{\mu}/\bar{\rho})$ and $z^* = z\cdot(\sqrt{\bar{\rho}\tau_w}/\bar{\mu})$. The relation for the semi-locally scaled quantities can be transformed to a relation for non-normalized ones. If the second term in the partial derivative of $z^*$ with respect to $z$, $\frac{\partial z^*}{\partial z} = \frac{\bar{\rho}\tau_w}{\bar{\mu}} + z\cdot\partial(\sqrt{\bar{\rho}\tau_w}/\bar{\mu})/\partial z$, which is vanishing at the wall and at the channel center, is neglected, the

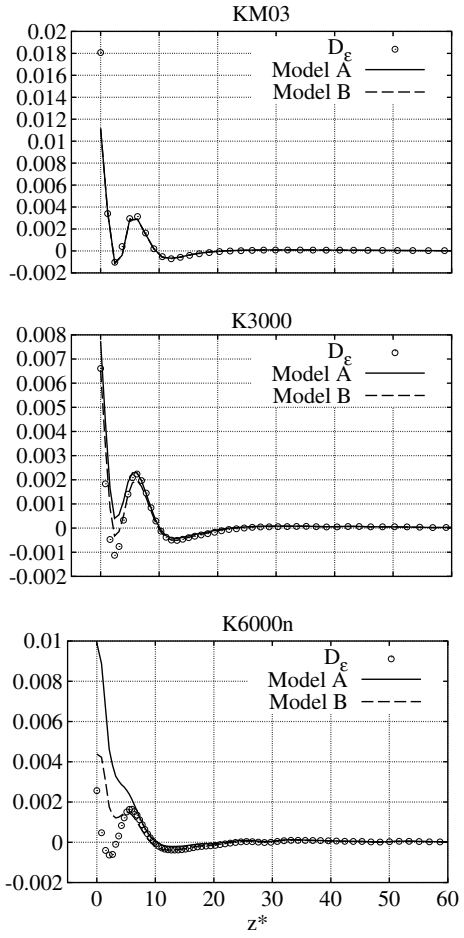


Fig. 9. Viscous diffusion term in the $\varepsilon_s$-equation, comparison between exact term and models in channel flow at different Mach numbers, semi-local scaling by $\tau_w^3/\bar{\mu}^2/\bar{\rho}$.

resulting model is $D_\varepsilon \approx [\bar{\mu}(\bar{\rho}\varepsilon\bar{\mu})_{,i}/\sqrt{\bar{\rho}}]_{,i}/(\bar{\mu}\bar{\rho}^{\frac{3}{2}})$ (Model B). In Fig. 9, both models and the exact term are shown. At low Mach number the models are indistinguishable. The second formulation gives better results, especially for high Mach numbers; although the behavior directly at the wall ($z^* < 3$) still cannot be captured exactly.

### 3.2. Mixing layer

The parameter range covered by the mixing layer simulation data is given in Table 2. Again, $Pr = 0.71$, $\gamma = 1.4$ and $\mu \sim T^{0.7}$. From this database, it is possible to investigate the effect of different Mach numbers (M10 and M11) and mean property variation (M10 and M14). The mean density difference in simulation M14 is the same as in the channel flow simulation at $M = 3.1$, K6000n, and $Re_\theta$ is the average Reynolds number over the time interval that was used to average the data using self-similar normalization. The box size and initial conditions are chosen as in the simulations described by Pantano and Sarkar (2002), but the spatial resolution is twice as fine in order to properly represent the dissipative range of wave numbers.

Table 2
Parameters of the DNS of time dependent mixing layers

| Flow case | $M_c = \frac{\Delta U}{c_1+c_2}$ | $\rho_2/\rho_1$ | $Re_\theta = \frac{\rho_{av}\Delta U\delta_\theta}{\mu_{av}}$ |
|---|---|---|---|
| M10 | 0.15 | 1 | 1072 |
| M11 | 1.1 | 1 | 984 |
| M14 | 0.197 | 2.7 | 941 |

The subscripts 1 and 2 denote the lower and the upper stream, $\delta_\theta$ the momentum thickness.

The mean velocity profiles are independent of Mach number. A density difference between the two streams causes the center of the mixing layer, identified by the peak in $K$, to be shifted continuously into the low density region as a result of mean momentum conservation. In simulation M14 the shift amounts to one momentum thickness. All profiles therefore become asymmetric. In order to compare the flows, data from M14 is always plotted over the shifted coordinate $z/\delta_\theta + 1$.

In the balance of the dissipation rate, $P_\varepsilon^1$ and $P_\varepsilon^2$ are not affected by either Mach number or density difference. However, $P_\varepsilon^4$ and $-\Upsilon$ vary under the different conditions, but their sum does not change substantially (see Fig. 10). The turbulent transport $T_\varepsilon$ was found to decrease with Mach number; however, the density difference causes it to rise at the low density side, reflecting the shift of the mixing layer (see Figs. 14–16).

The compressible term $T_\varepsilon^c$ and term $F_\varepsilon$ have positive non-zero values at the center in the case of high Mach number (M11), but they remain small compared to the other terms. The value of the baroclinic term $B_\varepsilon$ is even smaller.

However, in the mixing layer case with a notable density difference (M14), $B_\varepsilon$ becomes as big as $P_\varepsilon^1$ and has a similar shape. The compressible transport acts to redistribute the effects of dissipation from the high to the low density side. The term $F_\varepsilon$ is somewhat smaller and has an opposite effect (Fig. 11). $B_\varepsilon$ has to be modeled (see below), while the summed contribution of $F_\varepsilon$ and $T_\varepsilon^c$ still can be neglected.

The a priori tests using the mixing layer data can only give reasonable values for model coefficients in the inner

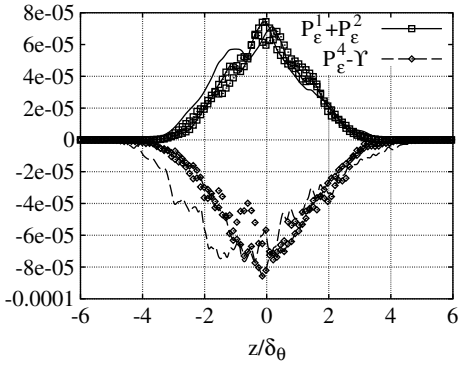


Fig. 10. Production and destruction terms in the $\varepsilon_s$-equation; mixing layers M10 (symbols), M11 (lines and symbols) and M14 (lines), scaling by $\Delta U^4/\delta_\theta^2$.

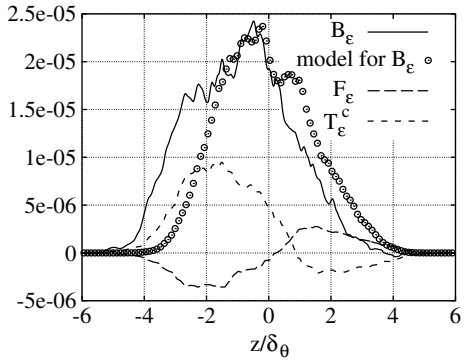


Fig. 11. Terms explicitly dependent on compressibility or density and viscosity gradients in the $\varepsilon_s$-equation; mixing layer with mean density difference M14, scaling by $\Delta U^4/\delta_\theta^2$.

part of the mixing layer, because at the edges both the exact terms and the modeled terms are much too small for meaningful comparisons. In the inner part of the mixing layer ($-3 < z^* < 3$), Fig. 12 shows that $C_\varepsilon^1$ is nearly independent of compressibility effects. There, the mean values and standard deviations are $0.66 \pm 0.05$, $0.72 \pm 0.06$ and $0.59 \pm 0.06$ for M10, M11 and M14. The value of $C_\varepsilon^2$ shows more irregularity, but the mean values of $1.11 \pm 0.22$, $1.20 \pm 0.09$ and $1.23 \pm 0.39$ for M10, M11 and M14 are close together (see Fig. 13).

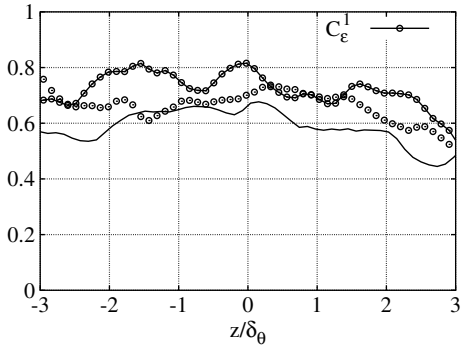


Fig. 12. Model coefficient $C_\varepsilon^1$; mixing layers M10 (symbols), M11 (lines and symbols) and M14 (lines).

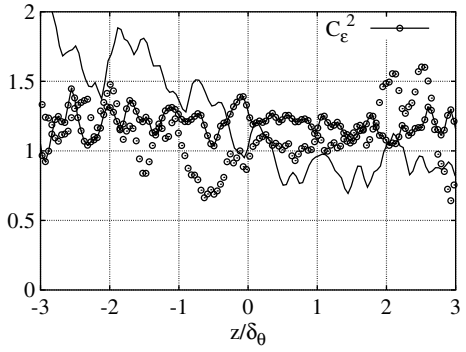


Fig. 13. Model coefficient $C_\varepsilon^2$; mixing layers M10 (symbols), M11 (lines and symbols) and M14 (lines).

Once again, the model for the turbulent transport term and the associated model coefficient are difficult to evaluate since $T_\varepsilon$ changes sign within the layer. It is more instructive to compare model and exact term directly. (Due to oscillations resulting from the evaluation of the terms in the model, a box filter with filter-width $\delta_\theta$ was used to smooth the profiles.) For all flow cases the agreement between model and exact term is good, if $f_t = 0.5$, as is shown by Figs. 14–16.

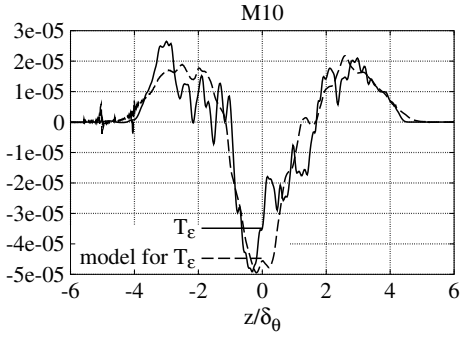


Fig. 14. Turbulent transport of solenoidal dissipation rate $T_\varepsilon$ and its model, $f_t = 0.5$; mixing layer M10, scaling by $\Delta U^4/\delta_\theta^2$.

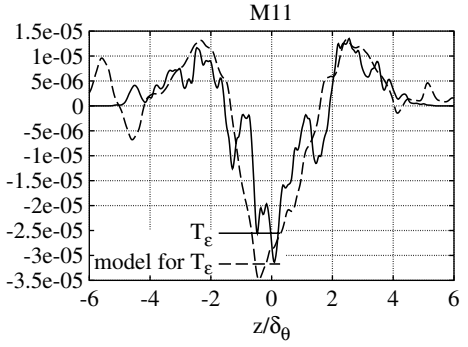


Fig. 15. Turbulent transport of solenoidal dissipation rate $T_\varepsilon$ and its model, $f_t = 0.5$; mixing layer M11, scaling by $\Delta U^4/\delta_\theta^2$.

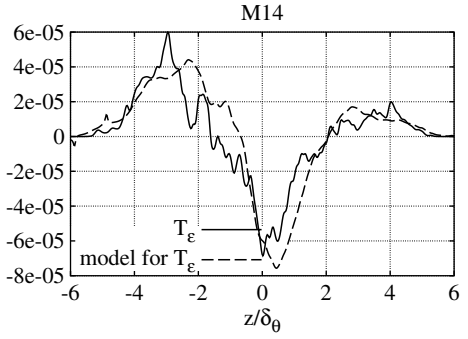


Fig. 16. Turbulent transport of solenoidal dissipation rate $T_\varepsilon$ and its model, $f_t = 0.5$; mixing layer M14, scaling by $\Delta U^4/\delta_\theta^2$.

Since the terms $P_\varepsilon^3$ and $D_\varepsilon$ are negligible in the mixing layer, models for these terms are not tested.

## 4. Modeling the baroclinic term

The model for $B_\varepsilon$ should fulfill the following conditions: (i) since it is only relevant in situations with mean density gradients, the model should include this factor; (ii) it should either scale as the other terms in the dissipation rate balance or vanish for infinite Reynolds number – otherwise no self-similar solution is possible. The model assumptions are checked using data from the mixing layer case M14.

At the outset, it has to be determined which correlation appearing in the term $B_\varepsilon = 2\tilde{\nu}\overline{(u'_{i,j} - u'_{j,i})\rho_{,j}p_{,i}/\rho^2} = -2\tilde{\nu}\overline{\vec{\omega}' \circ (\nabla p \times \nabla\rho)/\rho^2}$ has to be modeled. A first step is to treat the squared density in the denominator of the term:

$$\overline{\vec{\omega}' \circ (\nabla p \times \nabla\rho)/\rho^2} = \overline{\vec{\omega}' \circ (\nabla p \times \nabla\rho)}/\bar{\rho}^2 + \sum_{n=1}^{\infty} \overline{\vec{\omega}' \circ (\nabla p \times \nabla\rho) \cdot \left(-2\frac{\rho'}{\bar{\rho}} - \frac{\rho'^2}{\bar{\rho}^2}\right)^n}. \tag{12}$$

It can be shown from the DNS data, that the correlations with density fluctuations do not contribute substantially to the term.

Following Krishnamurty and Shyy (1997), the correlation in the first term on the RHS of Eq. (12) can be split into

$$\overline{\vec{\omega}' \circ (\nabla p \times \nabla\rho)} = \underbrace{\overline{\vec{\omega}' \circ (\nabla p' \times \nabla\bar{\rho})}}_{\text{Term 1}} + \underbrace{\overline{\vec{\omega}' \circ (\nabla\bar{p} \times \nabla\rho')}}_{\text{Term 2}} + \underbrace{\overline{\vec{\omega}' \circ (\nabla p' \times \nabla\rho')}}_{\text{Term 3}}. \tag{13}$$

These authors concluded from an order of magnitude analysis, that the second term is the dominant one. In a recent publication, Aupoix (2004) derived a model for the first term and neglected the remaining two. The present DNS data, however, leads to another conclusion. Fig. 17 shows, that the triple correlation (Term 3) dominates, which means, that this term has to be modeled.

The present modeling approach is to represent the scalar and vector products by rms-values and a correlation coefficient:

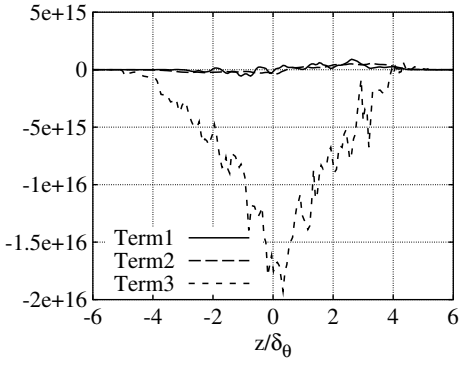


Fig. 17. Terms in Eq. (13); mixing layer M14.

$$\overline{\vec{\omega}' \circ (\nabla p \times \nabla\rho)} = \overline{\vec{\omega}' \circ (\nabla p \times \nabla\rho)'} \approx C \cdot \omega'_{\text{rms}} \cdot (\nabla p \times \nabla\rho)'_{\text{rms}}, \tag{14}$$

$$(\nabla p \times \nabla\rho)'_{\text{rms}} \approx C_{p\rho} \cdot \nabla p'_{\text{rms}} \cdot \nabla\rho'_{\text{rms}}. \tag{15}$$

In this approach, only $\omega'_{\text{rms}} = \sqrt{\varepsilon/\tilde{\nu}}$ is closed. $\nabla p'_{\text{rms}}, \nabla\rho'_{\text{rms}}$ and the coefficients $C$ and $C_{p\rho}$ have to be modeled.

It is assumed that the hydrodynamic pressure fluctuations $p'_{\text{rms}} \sim 2\bar{\rho}K$ are the relevant ones. Acoustic fluctuations are assumed not to contribute to the baroclinic term, since in a sound wave density gradients are parallel to pressure gradients. To get an estimate for the gradient, the relevant length scale has to be chosen. Using the assumption of isotropic turbulence and an inertial range, Batchelor (1951) estimated the fluctuating pressure gradient as $1.17Re_l^{\frac{1}{4}}2\rho K/l = 1.17 \cdot 2\rho K/\sqrt{l\lambda}$. In a later work, George et al. (1984) divided the fluctuating pressure gradient into a mean field–turbulence interaction part that dominates in the case of small Reynolds number, and a turbulence–turbulence interaction part. The first was modeled as $1.46S^*2\rho K/l$, and the second as $\sqrt{1.30Re_l^{1/2} - 50.832}\rho K/l$. For infinite Reynolds number, the model becomes $1.14Re_l^{\frac{1}{4}}2\rho K/l$, which is similar to Batchelor's estimate. According to these theoretical findings the model for $\nabla p'_{\text{rms}}$ has the form

$$\nabla p'_{\text{rms}} \approx C_p \cdot \frac{2\rho K}{\sqrt{\lambda l}} = C_p \cdot \frac{\rho\varepsilon^{3/4}}{\tilde{\nu}^{1/4}}. \tag{16}$$

The density fluctuations are estimated by a mixing length model. Since the mixing is affected by both the large and small scale structures, an intermediate length scale between the integral scale and the Taylor microscale would be appropriate. As the length scale for the gradient, the Taylor microscale is chosen, similar to velocity gradients.

$$\nabla p'_{\text{rms}} \approx C_p \cdot \frac{|\nabla\bar{\rho}|\sqrt{\lambda l}}{\lambda} = C_p \cdot |\nabla\bar{\rho}| \cdot \left(\frac{4K}{\tilde{\nu}\varepsilon}\right)^{1/4}. \tag{17}$$

Combining the results from Eqs. (14)–(17) yields the model

$$B_\varepsilon \approx 2C_{B_\varepsilon}\left(\frac{|\nabla\bar{\rho}|}{\bar{\rho}}\right)\sqrt{2K}\varepsilon. \tag{18}$$

It can immediately be seen that $B_\varepsilon$ is proportional to the mean density gradient as required by condition (i). Since in the mixing layer $\varepsilon \sim \Delta U^3/\delta_\theta$, $K \sim \Delta U^2$ and $\nabla\bar{\rho} \sim \bar{\rho}/\delta_\theta$, the complete model scales like $\Delta U^4/\delta_\theta^2$. This is the same scaling as the models for production, destruction and turbulent transport, so condition (ii) is fulfilled.

The assumptions associated with Eqs. (14)–(17) can be validated, and the model coefficients calibrated for the mixing layer M14 data. The a priori evaluation of the model given in Eq. (14) yields a value for $C$, the correlation coefficient between $\omega'$ and $(\nabla p \times \nabla\rho)'$. Fig. 18 shows the distribution across the layer. Its mean value for $-3 < z^* < 3$ is $-0.07$. Additionally, Eqs. (16) and (17) yield values for $C_p$ and $C_\rho$ of 3.1 and 1.2, respectively. Using these values,

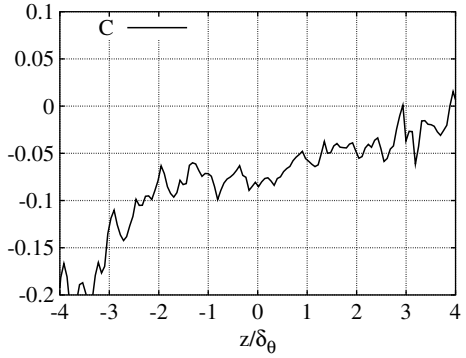


Fig. 18. Model constant $C$ (Eq. (14)); mixing layer M14.

Figs. 19 and 20 show the good performance of the submodels for fluctuating pressure and density gradients. The value for $C_p$ is roughly 2.5 times higher than the value predicted by Batchelor (1951) for high Reynolds number isotropic turbulence.

Writing the vector product in Eq. (15) in terms of the magnitude of the vectors and the angle $\phi$ between them gives

$$(\nabla p \times \nabla \rho)'^2_{\mathrm{rms}} = \overline{(|\nabla p'||\nabla \rho'| \sin\phi)^2} \approx C_{p\rho}^2 \overline{|\nabla p'|^2 |\nabla \rho'|^2}. \tag{19}$$

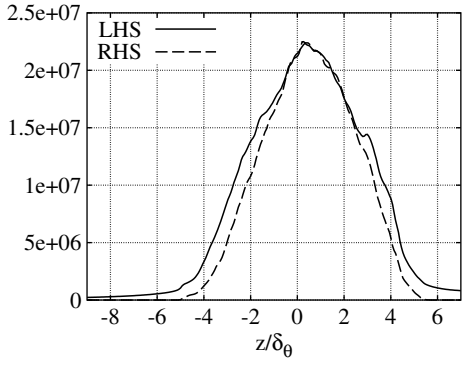


Fig. 19. Exact term and model for $\nabla p'_{\mathrm{rms}}$, Eq. (16), $C_p = 3.1$; mixing layer M14.

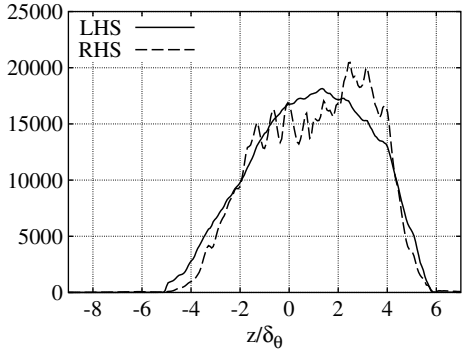


Fig. 20. Exact term and model for $\nabla p'_{\mathrm{rms}}$, Eq. (17), $C_p = 1.2$; mixing layer M14.

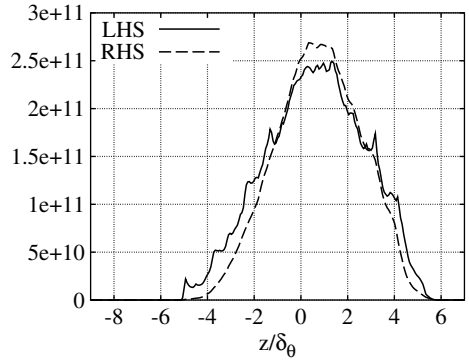


Fig. 21. Exact term and model for the vector product $(\nabla p \times \nabla \rho)'_{\mathrm{rms}}$, Eq. (15), $C_{p\rho} = 0.7$; mixing layer M14.

If it is assumed, that both the direction and magnitude of the gradients of pressure and density are uncorrelated, the above equation simplifies to

$$\overline{\sin^2 \phi} \approx C_{p\rho}^2. \tag{20}$$

The pdf $f(\psi)$ of $\phi$ needed to determine the value of $C_{p\rho}$ is $\frac{1}{2}\sin\psi$ under these assumptions.[2] So

$$C_{p\rho} = \sqrt{\int_0^\pi 1/2 \cdot \sin(\psi) \sin^2(\psi)\, \mathrm{d}\psi} = \sqrt{2/3} \approx 0.816. \tag{21}$$

Note, that the assumption of independence of the two vectors causes only their averaged vector product to be zero, not their rms-value.

This value slightly over-predicts the term in the mixing layer, but is close to the value of 0.7 determined from an a priori evaluation of the term (see Fig. 21). The assumption of independence of the gradients is not perfect, but does give a good estimate.

The comparison between the exact term $B_\varepsilon$ and its model using $C_{B_\varepsilon} = 0.18$ ($\approx 0.07 \cdot 0.7 \cdot 3.1 \cdot 1.2$) shows, that the model works well (see Fig. 11). Only the shift of the term into the low density region, in addition to the shift of the whole layer, is not correctly predicted since $C$ is taken as

[2] We are looking for the pdf of the angle $\phi$ between two independent vectors, which we consider as unit vectors. If the first vector is regarded as one axis of a sphere of radius $R = 1$, the second vector points from the center of the sphere to any point on its surface with equal probability. Now the probability $P$, that $\phi$ is smaller than a certain value $\psi$ equals the ratio between the segment of the surface of the sphere with $\phi < \psi$ and the whole surface of the sphere:

$$P\{\phi < \psi\} = \frac{\pi 2R^2(1 - \cos(\psi))}{4\pi R^2} = \frac{1}{2}(1 - \cos(\psi)).$$

So the probability density function $f$ is the derivative of $P$ with respect to $\psi$:

$$f(\psi) = \frac{1}{2}\sin(\psi).$$

constant (although its amplitude is rising towards the low density region, Fig. 18).

If the model is applied to channel flow at high Mach number, $B_\varepsilon$, which should be negligible, is overpredicted for $z^* < 30$. This is once again because $C$ is taken as constant, whereas it has a constant value of about $-0.08$ only for $z^* > 50$. Near the wall, it is close to zero. Additionally, very close to the wall ($z^* < 5$) the model cannot work, since there Term 1 in Eq. (13) dominates, because of the high mean density gradient.

## 5. Summary

An examination of terms in the solenoidal dissipation rate equation (5) shows added contributions from terms explicitly dependent on compressibility or density and viscosity gradients in addition to terms that also appear in incompressible flows. A new partitioning of these terms facilitates the identification of compressibility effects in the development of closure models for the terms explicitly dependent on compressibility or density and viscosity gradients as well as the standard terms appearing in both the incompressible and compressible formulations. The a priori analysis using DNS databases presented here leads to the following conclusions:

(i) Near cooled walls strong mean property variations are induced. The terms in the transport equation for the solenoidal dissipation rate are in most cases reduced by compressibility.

(ii) The tests show that the coefficients in the modeled terms of the solenoidal dissipation rate equation are independent of Mach number and mean property variation. It can be concluded that the compressibility effects in the transport equation for $\varepsilon_s$ are of indirect nature. This is reasonable, because compressibility effects should be proportional to the turbulent Mach number $M_t = u/c$ and the gradient Mach number $M_g = Sl/c$. Both parameters are related to large structures, and not to the small ones which predominantly determine the kinetic energy dissipation rate. The small structures scale with the Kolmogorov length $\eta$ and velocity scale $u_\eta$ and hence are very small. So the corresponding Mach numbers are close to zero and no direct compressibility effects are expected. Provided good incompressible models are available for all terms, their adapted forms will also be good models for compressible computations.

(iii) The relevance of the Mach numbers discussed in (ii) can also explain why the terms explicitly dependent on compressibility or density and viscosity gradients are negligibly small in most cases. In the only flow where these terms are of non-negligible size, the mixing layer with high mean property variation, this is not caused by high Mach number, but by low Mach number mixing of fluid of different density. For the baroclinic term $B_\varepsilon$ a model is proposed. The other two terms, $F_\varepsilon$ and $T^c_\varepsilon$, are not modeled, because their combined contribution can be neglected.

Even though these results are relevant to a wide variety of flows, the conclusions reached are not without limits. The compressible flows considered here were without shocks and without relevant changes of density or viscosity along a mean flow streamline. In flows where these phenomena appear, additional effects may arise and would have to be taken into account.

## References


Aupoix, B., 2004. Modeling of compressibility effects in mixing layers. J. Turb. 5, 007.

Batchelor, G.K., 1951. Pressure fluctuations in isotropic turbulence. Proc. Camb. Phil. Soc. 47, 359–374.

Blaisdell, G.A., Mansour, N.N., Reynolds, W.C., 1993. Compressibility effects on the growth and structure of homogeneous shear flow. J. Fluid Mech. 256, 443–485.

Coleman, G.N., Kim, J., Moser, R.D., 1995. A numerical study of turbulent supersonic isothermal-wall channel flow. J. Fluid Mech. 305, 159–183.

Foysi, H., Sarkar, S., Friedrich, R., 2004. Compressibility effects and turbulence scalings in supersonic channel flow. J. Fluid Mech. 509, 207–216.

George, W.K., Beuther, P.D., Arndt, R.E.A., 1984. Pressure spectra in turbulent free shear flows. J. Fluid Mech. 148, 155–191.

Hanjalić, K., Launder, B.E., 1972. A Reynolds stress model of turbulence and its application to thin shear flows. J. Fluid Mech. 52, 609–638.

Huang, P.G., Coleman, G.H., Bradshaw, P., 1995. Compressible turbulent channel flows: DNS results and modeling. J. Fluid Mech. 305, 185.

Kim, J., Moin, P., Moser, R., 1987. Turbulence statistics in fully developed channel flow at low Reynolds number. J. Fluid Mech. 177, 133–166.

Kreuzinger, J., 2006. Kompressibilitäts- und Dissipationseffekte in turbulenten Scherströmungen. Dissertation, TU München, Germany.

Krishnamurty, V.S., Shyy, W., 1997. Study of compressibility modifications to the $k$–$\varepsilon$ turbulence model. Phys. Fluids 9 (9), 2769–2788.

Mansour, N.N., Kim, J., Moin, P., 1988. Reynolds-stress and dissipation-rate budgets in a turbulent channel flow. J. Fluid Mech. 194, 15–44.

Nagano, Y., Shimada, M., 1995. Rigorous modeling of dissipation-rate equation using direct simulations. JSME Int. J., Ser. B 38 (l), 51–59.

Pantano, C., Sarkar, S., 2002. A study of compressibility effects in the high-speed turbulent shear layer using direct simulation. J. Fluid Mech. 451, 271–329.

Pirozzoli, S., Grasso, F., Gatski, T.B., 2004. Direct numerical simulation and analysis of a spatially evolving supersonic turbulent boundary layer at $M = 2.25$. Phys. Fluids 16 (2), 530–545.

Rodi, W., Mansour, N.N., 1993. Low Reynolds number $k$–$\varepsilon$ modeling with the aid of direct simulation data. J. Fluid Mech. 250, 509–529.

Sarkar, S., 1995. The stabilizing effect of compressibility in turbulent shear flow. J. Fluid Mech. 282, 163–186.

Simone, A., Coleman, G.N., Cambon, C., 1997. The effect of compressibility on turbulent shear flow: a rapid distortion theory and direct numerical simulation study. J. Fluid Mech. 330, 307–338.

Sinha, K., Candler, G.V., 2003. Turbulent dissipation-rate equation for compressible flows. AIAA J. 41 (6), 1017–1021.